Microelectronics Reliability 114 (2020) 113802

Contents lists available at ScienceDirect

Microelectronics Reliability

journal homepage: www.elsevier.com/locate/microrel

GaN-based high-periodicity multiple quantum well solar cells: Degradation under optical and electrical stress

A. Caria[a,*], C. De Santi[a], F. Zamperetti[a], X. Huang[b], H. Fu[b], H. Chen[b], Y. Zhao[b], A. Neviani[a], G. Meneghesso[a], E. Zanoni[a], M. Meneghini[a]

[a] Department of Information Engineering, University of Padova, via Gradenigo 6/B, Padova 35131, Italy
[b] School of Electrical, Computer and Energy Engineering, Arizona State University, Tempe, AZ 85287, USA

ABSTRACT

We investigate the degradation of InGaN-GaN MQW solar cells under optical and electrical stress. We submitted the devices to high temperature, high optical power stress and we found that, under optical stress, the devices show a moderate decrease in open-circuit voltage, possibly due to creation of defect-related shunt paths. This degradation is partially recovered after room temperature storage. The stronger decrease of open-circuit voltage under electrical stress at high current suggests a role of carrier flow in the degradation.

1. Introduction

The search for green alternatives to fossil fuels stimulates the research in the photovoltaics field. Silicon is the most used material to build solar cells, mainly because of its cost effectiveness, but has a limited absorption spectrum (especially in the blue and UV region), a relatively low Shockley-Queisser limit (30%). In addition, the temperature coefficient of silicon solar cells is rather high, meaning that their efficiency shows a measurable drop with increasing temperature. Multijunction solar cells reach efficiency up to 47% [1], being however difficult to build and very costly. Gallium nitride is a promising material for absorbing high-energy photons in multi-junction solar cells or also in Si-GaN tandem cells [2], with multiple quantum well (MQW) structures showing the best performance [3]. MQW cells showed various advantages over simple p-n or p-i-n junction structures, mainly due to the fact that is possible to grow thinner InGaN layer without incurring in dislocations and phase separation issues, typical of thick InGaN layers grown on GaN [4].

InGaN-GaN MQW structures has proven to be reliable also in harsh environments, under high excitation densities and at high temperature [5,6], enabling a possible use in wireless power transfer systems and space applications [7]. The aim of this work is to understand how MQW InGaN-based solar cells may degrade when submitted to high-power optical and electrical stresse at high temperatures.

2. Experimental details

The devices under test (DUTs, Fig. 1(a)) are grown by Metal-Organic Chemical Vapor Deposition (MOCVD) on a (0001) sapphire substrate. Over this substrate two Si:n-GaN (2 μm thick doping $3{\cdot}10^{18}$ cm^{-3}), and Si:n^{+}-GaN (125 nm thick, doping $2{\cdot}10^{19}$ cm^{-3}) layers are grown. On the top of these layers there is a periodic 30× GaN-$In_{0.15}Ga_{0.85}N$-GaN (7 nm/3 nm) structure, topped by Mg:p-GaN (100 nm thick, doping $2{\cdot}10^{19}$ cm^{-3}) and Mg:p^{+}-GaN (10 nm thick) layers. 1 × 1 mm^2 solar cells are built by standard lithography and processing. After the mesa etching, an indium-tin-oxide (120 nm thick) layer was deposed as current spreading layer. The cathode Ti/Al/Ni/Au contact and the anode Ti/Pt/Au contact were deposed respectively around the perimeter and on the top of the mesa [8].

We carried out dark and illuminated I–V characterization by means of a semiconductor parameter analyzer under 405 nm monochromatic excitation emitted by a laser diode. A beam sampler on the beam path deflects a small amount of the laser beam to a feedback photodiode to ensure that the intensity of the main beam is stable over time. The beam was attenuated by means of a series of optical filters, achieving characterization intensities ranging from 0.84 mW/cm^2 to 47 W/cm^2. The laser spot on the device was determined to have a nearly rectangular shape (1.4 × 0.15 mm^2) and was aligned along one diagonal of the device. The same 405 nm laser diode was used for the optical stresses with intensities up to 1200 W/cm^2. From illuminated I–V measurements we calculated the short-circuit current density J_{SC}, the open-circuit voltage V_{OC}, the external quantum efficiency at 405 nm EQE (i.e. the ratio between number of injected photons and extracted carriers) and the optical-to-electrical power conversion efficiency η_{OE} (i.e. the ratio between maximum electrical power and the optical power delivered to the cell). We also performed photocurrent spectroscopy

* Corresponding author.
E-mail address: alessandro.caria@dei.unipd.it (A. Caria).

https://doi.org/10.1016/j.microrel.2020.113802
Received 31 May 2020; Received in revised form 11 July 2020; Accepted 14 July 2020
Available online 01 November 2020
0026-2714/

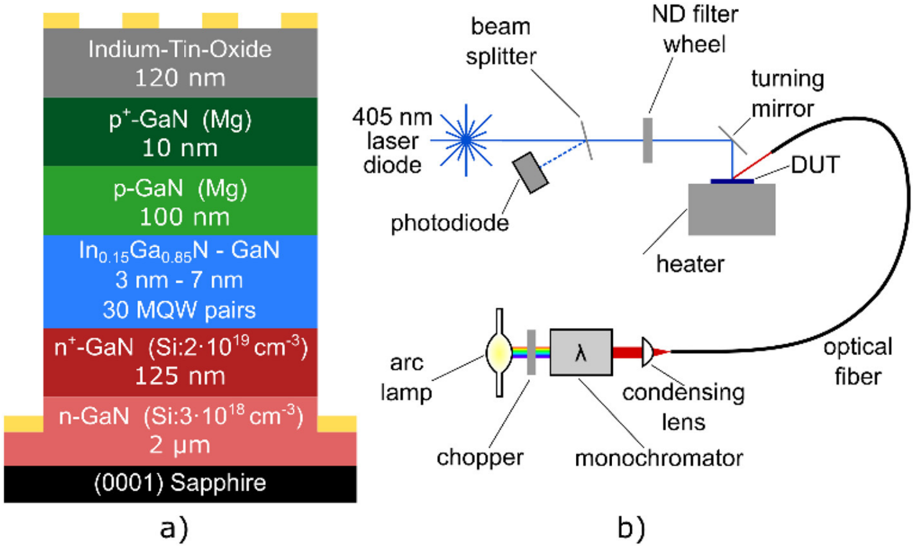

Fig. 1. Device structure (a) and experimental set-up (b).

measurements: the DUT was illuminated, under short-circuit condition, with chopped (f = 30 Hz) monochromatic light, emitted by a 300 W wide-spectrum Xenon arc lamp and monochromated by a grating monochromator. The photocurrent signal was amplified by a lock-in amplifier. This measurement allowed us to extrapolate the external quantum efficiency EQE under low excitation density in the range 280 ÷ 1100 nm. The DUT was heated by a ceramic heater, capable to reach temperatures up to 175 °C.

3. Results and discussion

We performed several stress tests to measure the device degradation under different optical power and current levels. We first performed an optical step-stress experiment, in which we submitted the DUT to an optical stress in short-circuit condition, increasing the stress optical power from 360.8 W/cm^2 to 1164.8 W/cm^2 in 30 min step at 100 °C baseplate temperature. The J_{SC} monitored during the stress (Fig. 2) shows that, by increasing the optical power, there is an increase in the photogenerated charge that can be extracted from the device, even if the excitation density levels are very high. In the last steps of the stress it is possible to see an increase (in absolute value) in the short-circuit current during the stress, that can be ascribed to the increase in

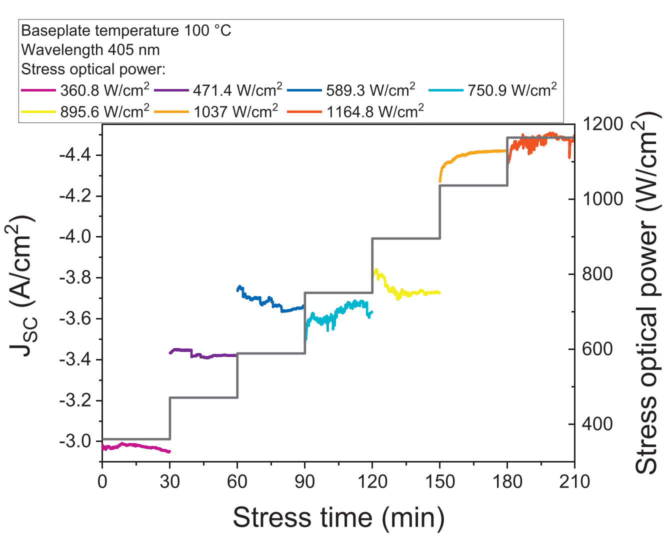

Fig. 2. Short-circuit current measured during optical step-stress.

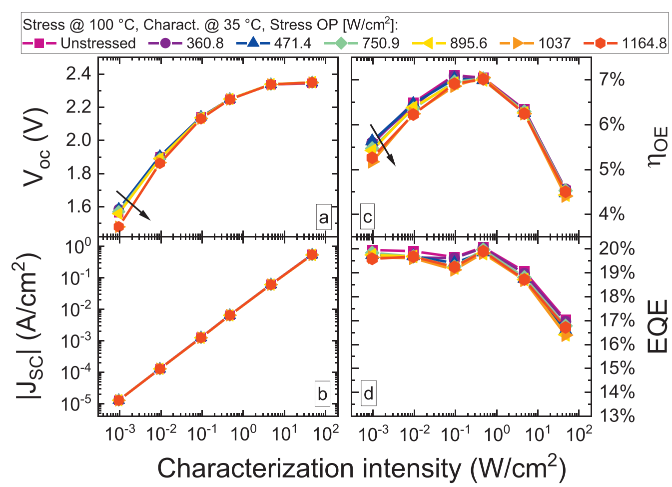

Fig. 3. Open-circuit voltage (a), short-circuit current density (b), optical-to-electrical conversion efficiency (c) and external quantum efficiency (d) measured at various excitation densities during optical step-stress.

thermionic escape from the wells due to device self-heating. After each stage of the stress tests, we characterized the device at 35 °C baseplate temperature, calculating V_{OC}, J_{SC}, η_{OE} and EQE (Fig. 3).

We observed negligible variation in J_{SC} and EQE, whereas we observed a slight decrease in V_{OC} and η_{OE} at the lowest characterization intensities. The decrease in open-circuit voltage can be ascribed to the creation of defect-related conductive paths in the active region of the device, possibly due to defect-related conduction, since they lower the V_{OC} mainly at low excitation densities and have no influence on the short-circuit current. This can be seen by considering a simple diode model with shunt resistance R_{SH}, which is described by the equation:

$$J = J_L - J_0 \exp\left(\frac{qV}{\eta k_B T}\right) - \frac{V}{R_{SH}} \tag{1}$$

where J_L is the photogenerated current density, J_0 is the saturation current density, q is the electron charge, η is the ideality factor, k_B is the Boltzmann constant and T is the temperature. In short-circuit current condition, V = 0 and $J_{SC} = J_L$, thus the shunt resistance does not affect the short-circuit current.

We then performed a temperature step stress, choosing an excitation density of 589.3 W/cm^2. In Fig. 4 the short-circuit current during the

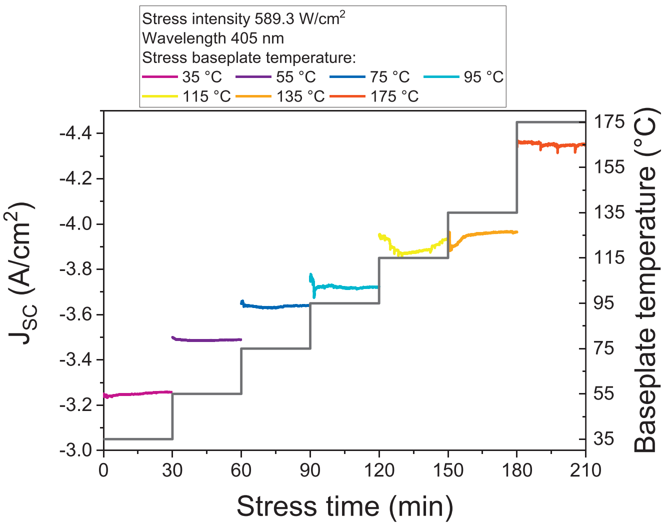

Fig. 4. Short-circuit current measured during temperature step-stress.

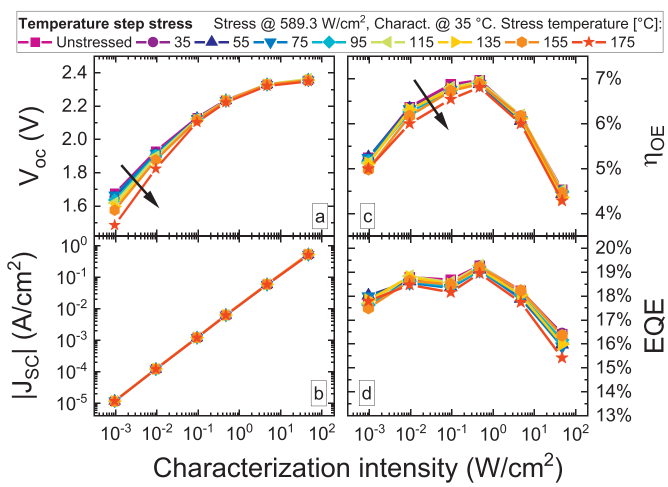

Fig. 5. Open-circuit voltage (a), short-circuit current density (b), optical-to-electrical conversion efficiency (c) and external quantum efficiency (d) measured at various excitation densities during temperature step-stress.

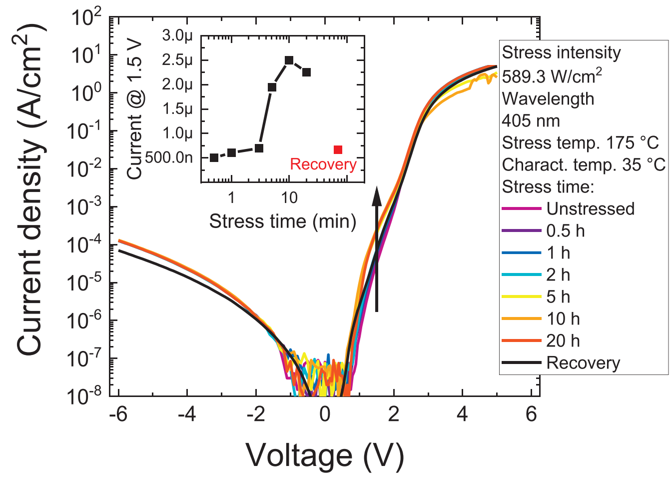

Fig. 6. Dark I–V characterizations during the constant optical power stress and after recovery (main plot) and current density at 1.5 V (inset).

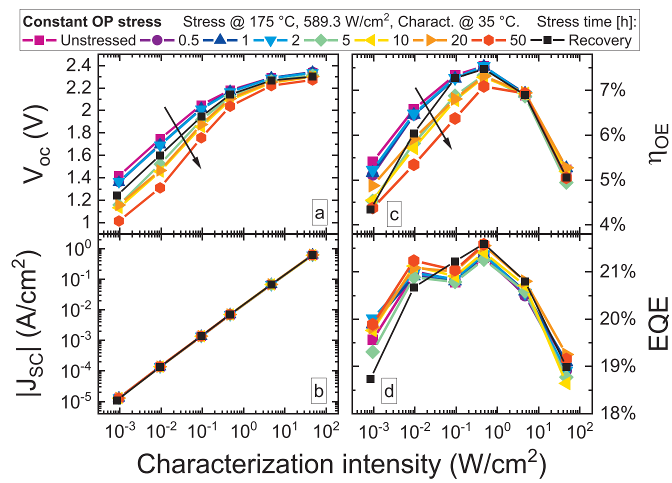

Fig. 7. Open-circuit voltage (a), short-circuit current density (b), optical-to-electrical conversion efficiency (c) and external quantum efficiency (d) measured at various excitation densities during constant optical power stress.

stress is showed. It is possible to see an increase in the J_{SC}, that can be ascribed to the increase in thermionic escape with increasing temperature, already observed in the optical step-stress. The operating parameters of the cells are showed in Fig. 5. Negligible degradation is visible in the short-circuit current and in the external quantum efficiency, whereas it is possible to see a degradation in the open-circuit voltage and in the power conversion efficiency, higher than the degradation seen in the optical step-stress: V_{OC} shows an average degradation of more than 3% with respect to the unstressed device (compared with the 1% of the optical step-stress), whereas the efficiency lowering is more than 4%, higher than the 2.5% reached during the optical step-stress.

In order to study the long-term degradation processes we choose an intensity of 589.3 W/cm^2 to perform a high-temperature (175 °C) constant optical power stress, based on the degradation data of the optical and temperature step stresses. After 52 days of storage (air, 25 °C) we performed new dark and illuminated I–V characterization to evaluate the recovery. In the dark I–V characterization (Fig. 6) we observed a slight increase in low forward bias current in the region between 1 and 2.5 V (see inset), possibly due to an increase in trap-assisted tunneling [9], that is partially recovered after storage.

We observed a reduction in V_{OC} and η_{OE} at the lowest characterization intensities (Fig. 7(a), (c)); this reduction was higher than the reduction seen in the optical step-stress experiment. We also observed negligible variation (less than 2%) in J_{SC} and EQE (Fig. 7(b), (d)), with no clear trend during the stress. The decrease in V_{OC} and η_{OE} was partially recovered after storage: the V_{OC} decrease after recovery (averaged at the various characterization intensities) with respect to the initial value was the 5% (being 13% after 50 h of stress), whereas the average conversion efficiency decrease after recovery was the 5% (being 10% after the stress). This behavior is possibly due to the creation of optically-induced metastable defects [10,11], causing an increase in tunneling, as noted by the dark I–V characterizations. Enhanced tunneling conduction acts similarly to a shunt in the region between 10^{-5} and 10^{-2} A/cm^2 (see again Fig. 6), thus causing the reduction in V_{OC} and η_{OE} seen at low excitation densities, whereas J_{SC} and EQE (that is calculated under short-circuit condition) are not influenced by it. This is the same mechanism that lowers open-circuit voltage and power conversion efficiency during optical (Fig. 3) and temperature (Fig. 5) step-stresses.

The photocurrent measurements (Fig. 8) show that the peak efficiency is around 405 nm, which matches the laser diode wavelength, whereas the absorption edge is around 460 nm, that is compatible with the 15% indium content. It is possible to see (inset of Fig. 8) the presence of an absorption edge around 550 nm, that can be ascribed to the presence of deep levels responsible for yellow luminescence in GaN, possibly due to carbon [12] or V_{Ga} complexes [13,14]. The yellow band

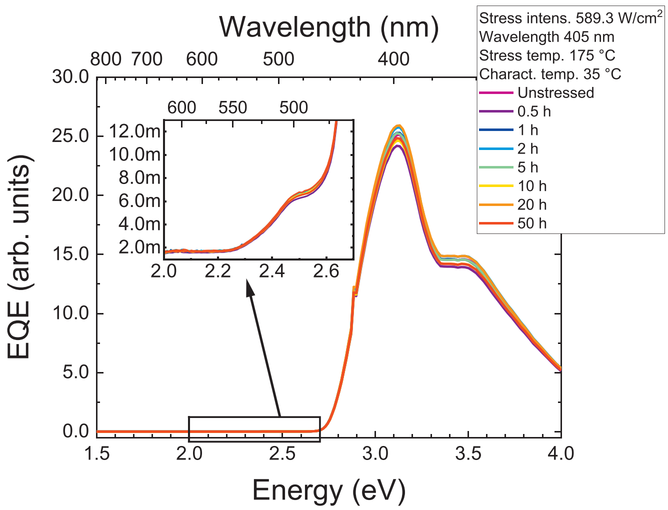

Fig. 8. Photocurrent spectroscopy measured during constant optical power stress.

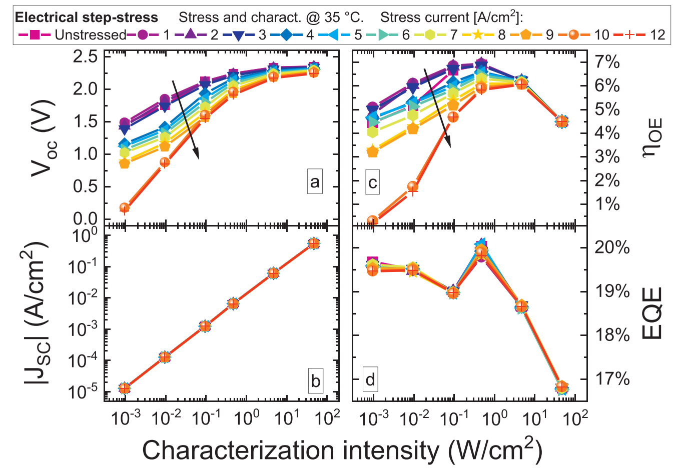

Fig. 10. Open-circuit voltage (a), short-circuit current density (b), optical-to-electrical conversion efficiency (c) and external quantum efficiency (d) measured at various excitation densities during current step-stress.

absorption efficiency does not change during stress, so there is no generation of new defects in this region and thus the defects responsible for degradation possibly have an activation energy are deeper than 2 eV, or are not detectable by photocurrent spectroscopy. Such states, with energies near the midgap or E_C-2 eV, are often related to parasitic conduction enhancement [15] and optical degradation, since they act as very efficient non-radiative SRH recombination centers [16].

In order to understand the effects of the flow of photogenerated carriers, we carried out an electrical stress on the device (i.e. no optical excitation was imposed on the DUT, that was stressed under forward bias condition), with current densities ranging from 1 A/cm^2 to 14 A/cm^2, when the device failed. From the dark I–V characterizations during the stress (Fig. 9) it is possible to see almost no degradation in the first steps of the stress, at current densities up to 4 A/cm^2. By increasing stress current, there is a degradation that is visible mostly as an increase in the current at low forward biases, between 1 and 2 V. This kind of degradation can be attributed to the increase in defects and the subsequent enhancement of trap-assisted tunneling in this voltage range [9]. The device degrades and fails as a short circuit for stress currents above 10 A/cm^2.

We also performed illuminated I–V characterizations during the stress, calculating the operating parameters of the cell (Fig. 10). At the

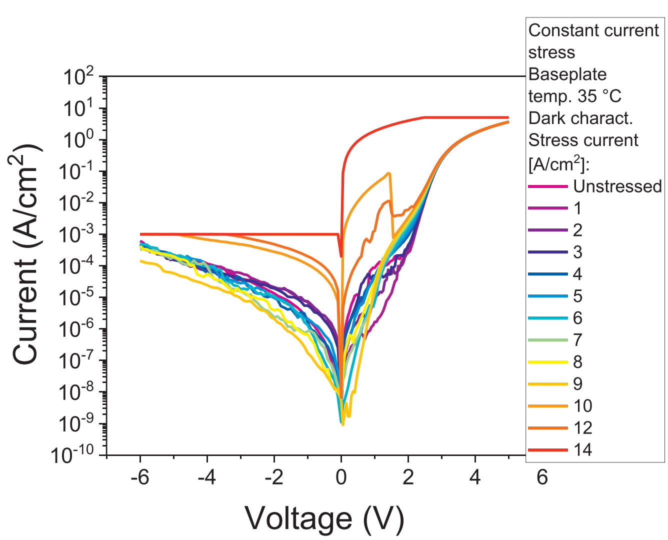

Fig. 9. Dark I–V characterizations of the device during electrical step-stress.

lowest current densities (1 ÷ 3 A/cm^2) the degradation is negligible and the operating parameters are stable. By increasing the stress current density we observe a significant degradation in V_{OC} and η_{OE}, that can be attributed to the enhanced defect-related forward conduction, whereas J_{SC} and EQE do not change. This effect is stronger at low excitation densities.

At very high current densities (12–14 A/cm^2) the device fails catastrophically as a short circuit. From this measurement we can hypothesize that the current flow could enhance the defect creation, causing the parasitic conduction of the device and the lowering of V_{OC} and η_{OE}.

4. Conclusions

In summary, we carried out optical and electrical stresses on InGaN-GaN MQW solar cells. The optical step-stress showed a very low degradation of the device, with a slight reduction in open-circuit voltage and power conversion efficiency at low excitation densities (on average, 1.3% and 2.5% respectively). A stronger degradation is observed during temperature step-stress up to 175 °C (3.3% and 4.3% for V_{OC} and η_{OE} respectively) and long term stress with an enhanced decrease in open-circuit voltage and power conversion efficiency, respectively 13% and 10%. The degradation during the long term stress is partially recovered after storage, finding a degradation of 5% for both V_{OC} and η_{OE} with respect to the unstressed device. The lowering in V_{OC} and η_{OE} is possibly related to the creation of parasitic conductive paths due to optically-induced metastable defects, with an activation energy lower than 2 eV. The results of the current step-stress suggest that the carrier flow can have a role in defect creation, since the degradation mechanism is similar to the mechanism observed during optical stresses.

Declaration of competing interest

The authors declare that they have no known competing financial interests or personal relationships that could have appeared to influence the work reported in this paper.

Acknowledgements

This research was partly performed within project INTERNET OF THINGS: SVILUPPI METODOLOGICI, TECNOLOGICI E APPLICATIVI, co-founded (2018–2022) by the Italian Ministry of Education, Universities and Research (MIUR) under the aegis of the “Fondo per il finanziamento dei dipartimenti universitari di eccellenza” initiative

(Law 232/2016).

References

[1] NREL Research Cell Record Efficiency Chart, https://www.nrel.gov/pv/cell-efficiency.html, (2020).
[2] N. Laxmi, S. Routray, K.P. Pradhan, III-Nitride/Si Tandem Solar Cell for High Spectral Response: Key Attributes of Auto-tunneling Mechanisms, Silicon, (2019), pp. 1–9, https://doi.org/10.1007/s12633-019-00342-y.
[3] R. Dahal, B. Pantha, J. Li, J.Y. Lin, H.X. Jiang, InGaN/GaN multiple quantum well solar cells with long operating wavelengths, Appl. Phys. Lett. 94 (2009) 063505, , https://doi.org/10.1063/1.3081123.
[4] M. Leyer, J. Stellmach, C. Meissner, M. Pristovsek, M. Kneissl, The critical thickness of InGaN on (0001)GaN, J. Cryst. Growth 310 (2008) 4913–4915, https://doi.org/10.1016/j.jcrysgro.2008.08.021.
[5] D.-H. Lien, Y.-H. Hsiao, S.-G. Yang, M.-L. Tsai, T.-C. Wei, S.-C. Lee, J.-H. He, Harsh photovoltaics using InGaN/GaN multiple quantum well schemes, Nano Energy 11 (2015) 104–109, https://doi.org/10.1016/j.nanoen.2014.10.013.
[6] J.-K. Sheu, F.-B. Chen, S.-H. Wu, M.-L. Lee, P.-C. Chen, Y.-H. Yeh, Vertical InGaN-based green-band solar cells operating under high solar concentration up to 300 suns, Opt. Express 22 (2014) A1222, https://doi.org/10.1364/OE.22.0A1222.
[7] C. De Santi, M. Meneghini, A. Caria, E. Dogmus, M. Zegaoui, F. Medjdoub, B. Kalinic, T. Cesca, G. Meneghesso, E. Zanoni, GaN-based laser wireless power transfer system, Materials (Basel) 11 (2018) 153, https://doi.org/10.3390/ma11010153.
[8] X. Huang, H. Chen, H. Fu, I. Baranowski, J. Montes, T.H. Yang, K. Fu, B.P. Gunning, D.D. Koleske, Y. Zhao, Energy band engineering of InGaN/GaN multi-quantum-well solar cells via AlGaN electron- and hole-blocking layers, Appl. Phys. Lett. 113 (2018), https://doi.org/10.1063/1.5028530.
[9] M. Mandurrino, G. Verzellesi, M. Goano, M. Vallone, F. Bertazzi, G. Ghione, M. Meneghini, G. Meneghesso, E. Zanoni, Physics-based modeling and experimental implications of trap-assisted tunneling in InGaN/GaN light-emitting diodes, Phys. Status Solidi 212 (2015) 947–953, https://doi.org/10.1002/pssa.201431743.
[10] S.J. Xu, G. Li, S.J. Chua, X.C. Wang, W. Wang, Observation of optically-active metastable defects in undoped GaN epilayers, Appl. Phys. Lett. 72 (1998) 2451–2453, https://doi.org/10.1063/1.121379.
[11] M.A. Reshchikov, H. Morkoç, Luminescence properties of defects in GaN, J. Appl. Phys. 97 (2005) 061301, , https://doi.org/10.1063/1.1868059.
[12] J.L. Lyons, A. Janotti, C.G. Van De Walle, Carbon impurities and the yellow luminescence in GaN, Appl. Phys. Lett. 97 (2010) 95–98, https://doi.org/10.1063/1.3492841.
[13] M. Asghar, P. Muret, B. Beaumont, P. Gibart, Field dependent transformation of electron traps in GaN p–n diodes grown by metal–organic chemical vapour deposition, Mater. Sci. Eng. B 113 (2004) 248–252, https://doi.org/10.1016/J.MSEB.2004.09.001.
[14] L. Stuchlikova, J. Sebok, J. Rybar, M. Petrus, M. Nemec, L. Harmatha, J. Benkovska, J. Kovac, J. Skriniarova, T. Lalinsky, R. Paskiewicz, M. Tlaczala, Investigation of deep energy levels in heterostructures based on GaN by DLTS, Eighth Int. Conf. Adv. Semicond. Devices Microsystems, IEEE, 2010, pp. 135–138, , https://doi.org/10.1109/ASDAM.2010.5666319.
[15] M. Auf der Maur, B. Galler, I. Pietzonka, M. Strassburg, H. Lugauer, A. Di Carlo, Trap-assisted tunneling in InGaN/GaN single-quantum-well light-emitting diodes, Appl. Phys. Lett. 105 (2014) 133504, , https://doi.org/10.1063/1.4896970.
[16] W. Shockley, W.T. Read, Statistics of the recombinations of holes and electrons, Phys. Rev. 87 (1952) 835–842, https://doi.org/10.1103/PhysRev.87.835.